TOWARDS MONOLITHICALLY PRINTED MFCS: DEVELOPMENT OF A 3D-PRINTABLE MEMBRANE ELECTRODE ASSEMBLY (MEA)

Pavlina Theodosiou[a], John Greenman[b] and Ioannis Ieropoulos [a,*]

[a] Bristol BioEnergy Centre, Bristol Robotics Laboratory, University of the West of England, Bristol BS16 1QY, UK

[b] Biological, Biomedical and Analytical Sciences, University of the West of England, BS16 1QY (UK)

* Corresponding Author: email: ioannis.ieropoulos@brl.ac.uk

Abstract

Additive manufacturing (3D-printing) and microbial fuel cells (MFCs) are two rapidly growing technologies which have been previously combined to advance the development of the latter. In the same line of work, this paper reports on the fabrication of novel membrane electrode assemblies (MEAs) using materials that can be 3D printed or extruded from the EvoBot platform. Materials such as air dry terracotta, air dry Fimo™ and standard terracotta were tested against conventional cation exchange membrane (CEM) material. The MEA was fabricated by painting the materials with custom made graphite coating. The results showed that the MFCs with the printable materials outperformed those using conventional CEM. Economic analysis showed that the utilization of ceramics-based separator can reduce significantly the overall costs. These findings suggest that monolithically printed MFCs may be feasible, as printable MEAs can improve MFCs performance, and help realise mass manufacturing at lower cost.

1. Introduction

Renewable energy production from waste using microbial fuel cell (MFC) technology is attracting growing attention as the ever-increasing worldwide energy demand is projected to increase 28% by 2040 [1]. MFCs are bio-electrochemical devices that use microorganisms as biocatalysts to convert chemical energy stored in organic matter into electrical energy, and date back to 1911 [2,3]. MFCs consist of two electrodes, a positive cathode and a negative anode, which are separated by a semi-permeable membrane or salt bridge [4]. Microorganisms are inoculated in the anodic compartment and anaerobically are capable of oxidizing the substrate. Frequently in MFC studies, anaerobic sludge effluents are used to inoculate the cells due to their very diverse microbial community presence [5], however microorganisms that can transfer electrons via metabolism to an external electrode can be also found in pond water and soil samples [6]. The electrons are released, via a process called extracellular electron transfer (EET), to the anode electrode either directly or indirectly (using mediators). The two electrodes are connected by an external circuit, which allows the flow of electrons from the anode side to the cathode side where the reduction of oxygen occurs. However, MFCs are not only considered as infinite-life biological batteries [7] but also as promising wastewater (WW) treatment solutions [8] which can complement or substitute the existing WW treatment technologies. The latter is due to the bacterial decomposition of the

41 organic matter or waste (eg. urine) in the MFC anodes which lowers the chemical oxygen
42 demand (COD) in the effluent even by 95% in real life field applications [9].

43 Electricity production, COD removal, cost and durability of MFC systems is largely affected by
44 and dependent on the materials used to build those units (or stacks) [10]. Anode materials
45 have to satisfy different requisites in order to be suitable for MFCs applications. The material
46 has to be electrically conductive, chemically and mechanically durable, low-cost and have high
47 surface area to enhance the bacteria-electrode interface. Carbonaceous materials certainly
48 are the suitable materials to fulfil these characteristics due to their cost efficiency and inertness
49 towards bacteria [11–13]. Hence materials such as carbon fibre veil [11], carbon cloth [14,15],
50 graphite felt [16,17] and carbon paper [18] have been extensively used in the MFC research.
51 Similarly, the cathode materials must possess specific characteristics [19,20] and ideally must
52 have high redox potential and the ability to readily capture protons in order to facilitate the
53 oxygen reduction reaction (ORR). Materials that fulfil those requirements
54 are carbonaceous materials and non-corrosive metals, same as those mentioned above
55 which are used as anode electrodes. Moreover, due to the sluggish ORR reaction occurring
56 at the cathode, a catalyst needs to be integrated within the cathode structure [21]. Due to that,
57 platinum group metals (PGM), platinum group metals-free (PGM-free) and metal-free high
58 surface area carbonaceous materials have been investigated in the past as catalyst [22].
59 However, PGM are expensive and have limited lifetime, as they are prone to
60 deactivation/poisoning reducing their activity and efficiency [23], therefore are not suitable for
61 MFC applications. PGM-free catalysts based on transition metals instead, are more reliable
62 and low cost compared to PGM. However, improvements are needed if they are to be
63 employed for large scale applications [22]. Metal-free high surface area carbonaceous
64 materials such as activated carbon have been recently heavily utilized with high durability, low
65 cost and commercial availability at large scale [9,24]. Another similar material which has
66 recently attracted an increasing interest due to its biocompatibility and economical nature, is
67 the bamboo charcoal granules and tubes [25–27]. Lastly a material that plays a crucial role in
68 high power performances is the current collector which is usually of the same nature as the
69 electrode or can be a different material such as stainless steel mesh which provides
70 mechanical strength and is corrosion proof [28].

71 In parallel, membrane materials are an important element within the microbial fuel cell system.
72 Polymeric separator based on Nafion or Nafion-derived fluorinated polymers are considered
73 the bottleneck of the MFC research and the main contributor to high cost and internal
74 resistance [29]. Additionally, those types of membranes are prone to biofouling after long term
75 operation (more than 60 days) [30,31] which is a result of microorganisms, microbial
76 extracellular polymers and salts depositing on the membrane. This, along with possibly contact
77 resistance, impacts negatively the MFC power performance (up to 37% decrease) due to the
78 deterioration of the cation transfer which limits the charge transfer and increases the systems'
79 internal resistance (up to 20%) [32]. Moreover, in the open-to-air configuration, the cathode is
80 often not well integrated within the membrane, therefore the contact resistance is even higher,
81 and output is limited. To overcome these issues, alternative MFC architectures and materials,
82 such as ceramic based [33,34], need to be identified (or examined further) as well as ways to
83 manufacture and integrate them. One possible design that can benefit the system is the
84 integrated membrane electrode assembly (MEA) in which the cathode is built on the
85 membrane itself. It was previously shown that the power output is improved by reducing the
86 internal resistance [35].

87   MEA is the assembled system comprised of a membrane and an electrode/s attached together
88   as one through pressing with or without heat treatment in order to minimise the distance
89   between them. This arrangement has been inherited from traditional chemical abiotic fuel cell
90   and showed higher power densities compared to the conventional separated membrane and
91   electrode configurations [35]. However, only a few studies have focused on MEA influence on
92   MFC systems and even fewer on 3D-fabrication techniques to manufacture these MEAs.

93   The present study looks at 3D printing MFCs using novel extrude-able materials that can be
94   produced from the EvoBot platform; a Rep-Rap 3D printer turned to robot which can inoculate,
95   maintain and print parts for MFCs [36]. The focus is on the development of cost-effective MEAs
96   using extrude-able air-dry membranes coated with conductive paint. Different ceramic and
97   polymeric based membranes were investigated and compared in terms of chemical
98   composition and properties. The electrical conductivity, surface morphology and chemistry of
99   the materials were also analysed. At last, the electrochemical performance in terms of power
100 generation was measured and reported.

101 ## 2.   Materials and Methods

102
103 ### 2.1 Membrane Materials

104 For the scope of this experiment, three types of potentially extrude-able membranes were
105 tested and compared against a conventional cation exchange membrane (CEM) (Membranes
106 International, USA). The materials tested were Fimo™ air-dry clay (Staedtler, German),
107 terracotta air-dry clay (Hobbycraft, UK) and red terracotta modelling clay (Tiranti, UK). The
108 latter was kilned at a temperature of 1070°C prior to use, to allow the structural bonding of the
109 clay and ensure durability, whereas the other two were dried overnight at room temperature.
110 All three membranes were prepared using the same process as previously described [37] and
111 the thickness of the tested membranes was consistent for all the custom made membranes
112 (2.5mm). The total surface area of the membranes was 25 cm^2. The control (CEM) membrane
113 required activation in 5% NaCl at 40°C for 12 hours prior to use. The images of the different
114 membranes utilised in this study are shown in Figure 1.

115 ### 2.2 Membrane electrode assembly

116 A conductive graphite coating was applied to each membrane and formed the cathode
117 electrode. The coating was fabricated using polyurethane rubber coating (PlastiDip), white
118 spirit and graphite powder as previously described [38]. The membranes were coated
119 uniformly with the conductive cathode mixture using a brush followed by the Dr. Blade
120 technique using a spatula. The surface resistance was measured during each coating (Section
121 2.3.4). After the membrane electrode assembly had dried, a cable was attached to the cathode
122 using conductive wire glue, to form the cathodic current collector.

123

124 ### 2.3 Characterization of membrane and electrode

125
126 ### 2.3.1   Chemical composition of the membranes

A qualitative chemical analysis of the membranes was determined using the Oxford Instruments Aztec energy dispersive X-ray (EDX) system and the main elemental content of each membrane sample was identified.

2.3.2 Morphology of the electrode

Surface morphology of the electrode side of the MEA was acquired through images using FEI Quanta 650 field emission scanning electron microscopy (SEM) at difference magnifications.

2.3.3 Hardness test

The hardness of the membranes materials was tested using the Vickers Hardness Testing equipment [39] (Buehler, UK). Particularly; the entire 25 cm^2 of the membrane was used for the hardness testing. Average values were obtained from five readings taken from five different locations on the membrane and located 5 cm apart.

2.3.4 Electrical conductivity of the cathode multiple layers

The in-plane conductivity of the cathode was measured through a handheld digital multimeter (TENMA, 72-7750). Particularly, crocodile clips were attached on the opposite sides of the membrane electrode assembly and the resistance was measured. This operation was repeated for each layer of graphite applied on the membrane. This method was only used to give an early indication of the in-plane resistance of each conductive coating addition.

2.4 MFC architecture

Four triplicates of analytical size MFCs were assembled for this experiment. Each MFC consisted of a single chamber with an empty volume of 25 mL in which the anode was inserted. The MFCs were constructed using one side of a covered 15mm thick Polymethyl methacrylate (Perspex) sheet. The anode electrode was a folded carbon veil fibre (20gm^{-2} carbon loading) with a projected area of 8.45 cm^2 and total surface area of 270 cm^2 (PMF Composites, Dorset, U.K.). The cathode was integrated with the four different membranes and directly glued to the anode chamber with an inert aquatic sealant (Aquabits, UK). In order to maintain the moisture of the membrane electrode assemblies and maintain a liquid 'bridge' for proton transport, the MFCs were wrapped with Parafilm® which is a highly waterproof material but at the same time is permeable to oxygen (Figure 1.A).

2.5 Inoculation and feedstock

The twelve MFCs were inoculated with a mixture of 50% fresh human urine collected anonymously from healthy individuals and 50% anolyte derived from already established experiment operating on activated sludge (Wessex Water, UK) and urine. The mixture was enriched with a background solution of TYE which was comprised of tryptone (1%) and yeast extract (0.5%) as nutrient and amino acid supplier. The solution was left in a shaking incubator (Orbital Incubator S150) for 24 hours at a shaking speed of 130 rpm and at a temperature of 36.6°C. The solution was transferred to 15 mL centrifuge tubes (Corning, UK) and placed into the centrifuge (VWR Compact Star CS4) for 10 minutes at 5000rpm. Subsequently, the supernatant was removed and the pellet re-suspended into 5 mL of neat urine. The re-suspended medium was collected and formed the inoculum for the experiment. After inoculation period when the biofilm formed, the MFCs were fed manually in batch mode with

167 urine. The experiment was performed at room temperature (22 ± 2 °C) within a temperature-
168 controlled environment.

2.6 External resistance and polarization experiment

170 The MFCs operated in a fixed load of 2.7 kΩ prior to polarization experiment, which was
171 conducted on the MFCs by connecting them to 8-channel automated *Resistorstat* equipment,
172 developed as described in Degrenne *et.al.* [40]. The external resistance ($R_{ext.}$) was ranging
173 decreasingly from 30 kΩ to 3.74 Ω with each resistance value held for 3 minutes. During
174 polarization, voltage output was recorded every 30 s (6 samples per resistance value) to make
175 it possible to monitor and capture the dynamic response of MFC to changes in $R_{ext.}$. The MFCs
176 were kept in open-circuit voltage for 2 hours prior to polarization testing. Following the first
177 polarization experiment the R_{ext} was changed to 1 kΩ, a value at which maximum power was
178 generated. This load was kept constant until the end of the experiment.

2.7 Data recording and calculations

180 The MFCs were individually connected to an Agilent Keysight 34970A Data Acquisition / Data
181 Logger Switch Unit (Keysight Technologies, UK) for data recording of voltage (mV) against
182 time with readings taken every 3 minutes. The data were processed and analysed using MS
183 Office Excel where current (I) in amperes (A) was calculated in accordance with the Ohm's
184 Law; I = V/R, where V is the measured voltage and R is the known value of the external
185 resistive load in ohms (Ω). Power (P) values in watts (W) were calculated by multiplying
186 voltage with current: P = I x V [41].

2.8 COD measurements

188 Chemical oxygen demand (COD) removal analysis was carried out on the forty-second day of
189 the experiment by analysing the influent sample and comparing it with the effluent sample
190 after 24 hour retention time in the MFC. The analysis were conducted using the potassium
191 dichromate oxidation method (CamLab, UK) with high range (HR) COD vials in which 0.2 mL
192 of sample to be analysed (inlet and outlet) was taken from the MFC and filtered before being
193 added into the vial. The sample was then heated up at 150°C for 2 hours and cooled down for
194 another 2 hours. At last, the concentration was measured through a spectrophotometer
195 (Lovibond Water testing).

2.9 Breakdown of the experimental procedure

197 The experimental plan that was followed in this study has been summarised and presented
198 at Table 1. The table notes in detail the feeding regime followed, the operational conditions,
199 urine replacements, timings and quantities of feedstock as well.

Breakdown of the experimental scheme			
Day 0	Inoculation	100% inoculum	Full exchange (25 mL)
Day 1-2	Inoculation	50% inoculum – 50% urine	Full exchange (25 mL)
Day 3-4	-	No feeding	-
Day 5-9	Daily Feeding	100% urine	Full exchange (25 mL)
Day 10-14	Daily feeding	100% urine	5 mL top-up

Day 15 onwards feeding regime: a complete exchange of anolyte early each week, followed by a daily top-up of 5 mL until the end of the week.

|			
Day 15-25	Daily feeding	Water diluted urine	Feeding regime described above
Day 26-30	Daily feeding	100% urine	Feeding regime described above
Day 30	Polarization	Change of Rext. from 2.7 kΩ to 1 kΩ	
Day 31-58	Daily feeding	100% urine	Feeding regime described above
Day 59-62	Starvation period	No feeding	-
Day 63-73	Daily feeding	100% urine	Feeding regime described above

Table 1. Breakdown of the experimental scheme followed through the entire duration of the experiment.

200

201   **3. Results and Discussion**

202

203   **3.1 Material selection**
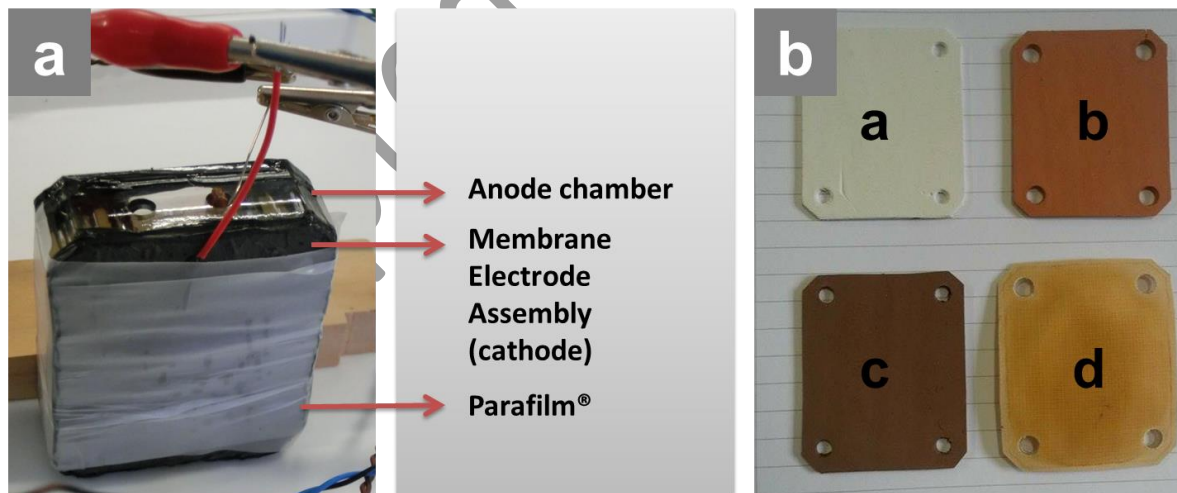
Figure 1. Photographs of a) the MFC set-up and b) the four cut-to-shape membrane materials Air-dry Fimo™ (a), Air-dry Clay (b), Terracotta (c) and Cation exchange membrane (d).

204   Four different membranes (Figure 1.B) were selected and investigated as separators in MFCs
205   fed with urine. Two of the membranes were based on air-dry techniques and were Fimo™ air-
206   dry clay and terracotta air-dry clay. These two materials were selected due to the advantage
207   of being extrude-able from an adapted 3D-printer nozzle, which can be incorporated in the
208   EvoBot platform. Furthermore, the air-drying technique allows fabricating ceramics just

209　through normal atmospheric conditions without the utilization of heat treatment. Red terracotta
210　modelling clay was another membrane used for this experiment and acted as a control to the
211　investigation. However terracotta was subject to high temperature treatment in controlled
212　atmospheric conditions which allowed the internal binding of the clay within the structure as
213　needed [37]. The last membrane utilized was a commercial polymeric-based cation exchange
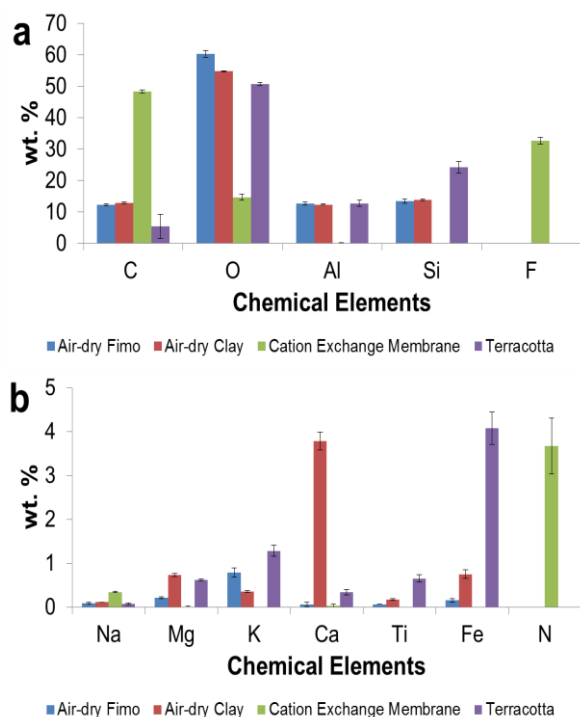214　membrane.

215　**3.2 Material analysis**
216　**3.2.1　Chemical composition of the membranes**

217　Energy dispersive X-ray (EDX) system was used for the qualitative chemical analysis of the
218　elements composing each membrane tested during this investigation. C, O, Al, Si and F were
219　the elements identified with percentages above 10% (Figure 2.A). Carbon and oxygen were
220　detected in all four samples, however it is notable that aluminium and silicon were detected
221　only for the ceramic-based membranes. These elements are well known to be generally
222　integrated within ceramic materials especially in their oxide form [42]. As expected fluoride
223　was only detected in the polymeric membranes. Generally, polymeric membranes are
224　composed by a backbone of fluorinated polymer that gives mechanical strength and resistance
225　to harsh and corrosive environments. Unfortunately, F is not environmentally friendly and
226　therefore the utilization of fluorinated materials in microbial fuel cells might negatively impact
227　the environment after long terms operations. In fact, if those MFCs are to be used on-board
228　low-power robots that are programmed to perform a particular task and then degrade naturally
229　in the environment [43] then the use of fluorinated membranes needs to be avoided.

230　Additionally, elements with percentage lower than 5% were also reported (Figure 2.B). Traces
231　of Na, Mg, K, Ca, Ti and Fe were detected within the ceramic-based samples. Only Na and N
232　were detected on the polymeric membrane. Interestingly, a percentage of ~3.5% of Ca was
233　measured in the air-dry clay and higher content (roughly 4%) of iron was detected in the
234　terracotta sample.

235

Figure 2. ED-X analysis results data of the chemical elements between the four tested types of membranes. a) Major and minor components b) trace elements.

236

3.2.2 Morphology of the electrode

238 The morphology of the graphite-based coating was observed using SEM images at different
239 magnifications (Figure 3). Increasing magnifications allowed visualising the surface of the
240 electrode in more detail. The surface of the electrode in fact seems to be fully covered by a
241 quasi-uniform coating. At higher magnification, the graphite particles could be clearly detected
242 with non-uniform shape and length within the micrometric shape in agreement with the
243 manufacturer's specifications [44].
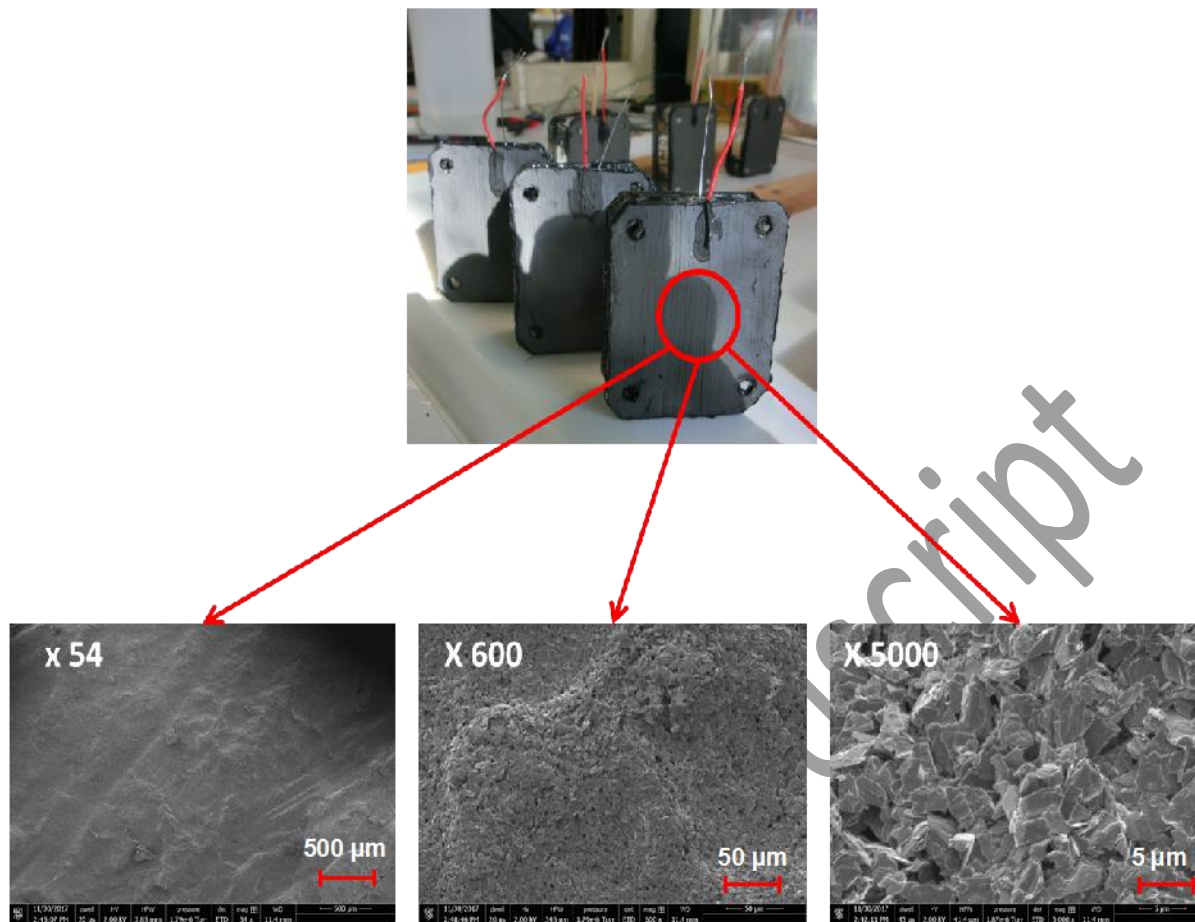
Figure 3. SEM images at three different magnification of the MEA side surface coated with the graphite ink (cathode side).

3.2.3 Electrical conductivity of the cathode multiple layers

The MEAs were prepared by applying the conductive ink directly on to the already set membranes using a layer-by-layer technique akin to a 3D-printer approach. Each layer was left to air-dry before each in-plane measurement of resistance was taken. Figure 4.A. shows the in-plane resistance of the air-dry clay and terracotta clay based MEAs after applying the first, second and third layer of conductive ink on their surfaces. Those two sets of data were chosen to be discussed as they illustrate nicely the initial difference in resistance between the two differently made clays (air dry and kilned). Initially the terracotta MEA had almost 2.5 x higher resistance compared to air-dry clay. The difference in resistance became larger after applying the second layer of coating with terracotta being 5.0 x higher that air-dry clay even though the overall resistance decreased for both by nearly 2.0 x and 4.0x respectively. Despite the differences and high resistance values initially, by the time the third layer of conductive coating was applied and cured, both MEAs showed similar in-plane resistance (170±5 Ω). This suggested that by that time the conductive ink coating covered completely the surface of the membrane and bonded with the underlined layers of coating in a quasi-uniform manner, in agreement with the SEM micrographs. It is noteworthy that in an attempt to decrease the in-plane resistance even more, a fourth layer of coating was applied on the membranes however this had an adverse effect on the continuity of the electrode as it caused cracking of the upper layer of coating (data not shown). Thus for the scope of this experiment only three layers of coating were applied on each membrane and form the MEA, which was in

264 accordance to what has been reported in the literature for similar conductive inks applied on
265 paper-based MFCs [45]. Following the application of three consecutive layers of conductive
266 ink on the MEAs the in-plane resistance values were measured and plotted on Figure 4.B
267 showing that all MEAs had an overall resistance of 150±15 Ω. More specifically, Fimo™ had
268 an in-plane resistance of 135 Ω followed by CEM with a resistance of 143 Ω, air-dry clay and
269 terracotta as mentioned above had a similar resistance of 158 and 168 ohms, respectively.
270 These results have given an initial indication of the in-plane resistance after each layer of
271 graphite coating, which can provide information on the current connecting losses of the MEA.
272 In further investigation of MEA materials, through-plane resistance it is recommended to be
273 measured in order to provide more comprehensive results on the whole MEA resistance.

274
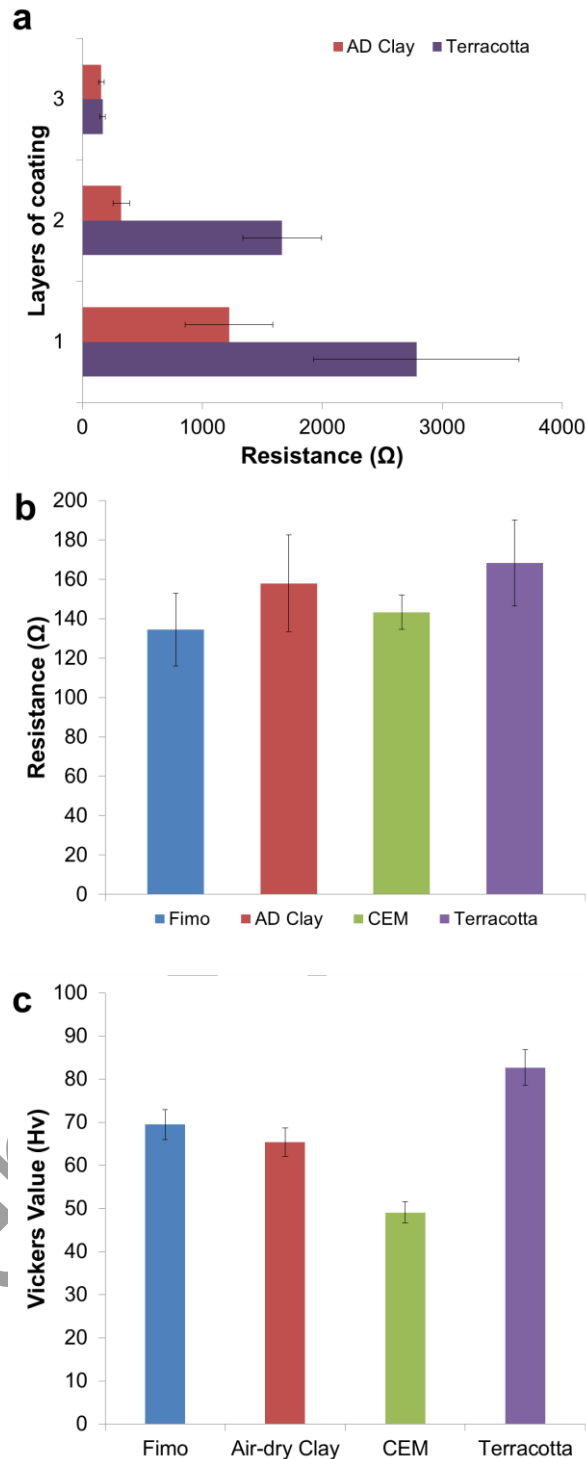
Figure 4. Resistivity of the MEA and hardness of the membrane. a) average resistance values after each coating on the membrane b) average surface resistance of the MEA electrode c) hardness test based on Vickers value (Hv).

275 It is well known from the literature that ceramics possess many unique characteristics that
276 make them suitable for use within MFC systems; one of these advantageous characteristics
277 is their structural durability [33]. In order to test the durability of the materials under
278 investigation against terracotta, a Vickers hardness test was performed. Even though this
279 technique is well used for testing metal materials, it has been reported in the past that it can
280 be used for ceramic materials [39] to give an indication of durability between different samples.

281 The unit of hardness given by this test is the Vickers Pyramid Number (HV), the five values
282 obtained from each ceramic testing were averaged and presented in Figure 4.C. The results
283 confirmed that terracotta was indeed the most durable/hardest (82.7 HV); however air-dry
284 Fimo™ and air-dry clay were only 13 and 17 HV units more fragile, respectively. To put the
285 results into perspective a diamond has a hardness value of 10000 HV. Those data are an
286 early indication that even though air-dry clays are not as structurally robust as kilned terracotta,
287 they can still be proven to be durable. The hardness of the materials was tested in order to
288 observe the properties of the material in question, in terms of deformation from a standard
289 source (the metal indenter), which would in turn provide an indication of the material's ability
290 to resist wear, pressure, or damage, which is particularly relevant for shipping systems like
291 these to other areas.

292 ### 3.3 Power Output
293 ### 3.3.1 Initial power output profile of the first fifteen days

294 For this experiment, MFCs using different membrane materials were tested with the ultimate
295 aim to observe the feasibility of using air-dry clays that can be 3D-printed, as separators for
296 MFCs. As previously mentioned (Section 2.5), the MFCs were all inoculated with a mixture of
297 activated sludge, tryptone yeast extract and effluent from established urine fed MFC
298 experiments. After inoculation, the MFCs were left in open circuit for three hours until the
299 voltage plateaued. The observed potential difference between the anode and cathode from all
300 the MFCs was roughly 600 ± 50 mV (data not shown). An external load of 2.7 kΩ was connected
301 on all MFCs, closing the circuit and initiating the power generation process by encouraging
302 the formation of an electroactive biofilm on the anode electrode. The MFCs were maintained
303 in a batch fed mode. Each feeding can be simply identified on the graph as every time a
304 feeding occurred, an instant increase -followed by gradual decrease- in power output can be
305 observed. This is reflected by the fact that the energy source availability within the anode
306 chamber increased, meaning that bacteria have fresh and available organic matter to
307 metabolise. The first two exchanges in anolyte consisted of replenishing fully the chamber with
308 the aforementioned inoculum and urine in a 50%:50% ratio, which was sufficient to supply the
309 bacteria with the much needed carbon energy sources to continue their metabolic activities
310 during "periods of no feeding", which were beyond the normal feeding cycle (Figure 5). During
311 this period, the MFCs with air-dry clay membrane decreased in performance by 13.2%, which
312 was similar with the air-dry Fimo™ (13.8% decrease). The MFCs with terracotta and CEM
313 were the most affected showing a decrease of 18.6% and 40.0% respectively.
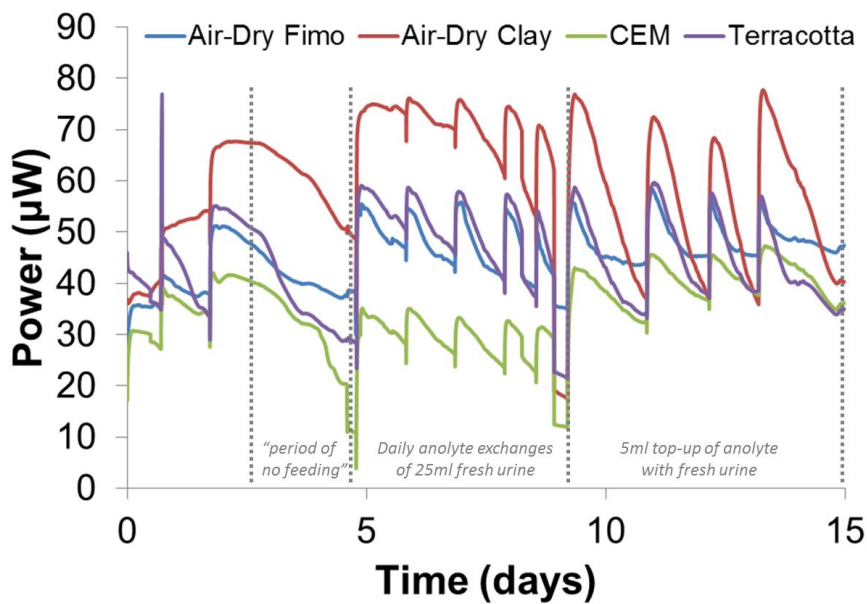
Figure 5 Power generation recorded in the first 15 days of operations.

314

315   On the fifth day, the anode chamber of each MFC was replenished completely (25 mL) with
316   fresh urine that resulted in increasing the power output by 14.4% and 14.8% on the air-dry
317   clay based MFCs, 29.7% for the CEM based MFCs and nearly 50% in the terracotta based
318   MFCs (Figure 5). It is assumed that the terracotta based MEA had the greatest improvement
319   in power following carbon-energy depletion, because of the higher porosity compared to the
320   other materials, which has a direct impact on the cation rate of exchange. Higher porosity, and
321   non-selective materials will naturally allow a higher rate of cations to diffuse through – a
322   process which is driven by electron-neutrality. This means that for selective or lower porosity
323   materials even if the rate of electrons generated by the biofilm communities is at similar levels
324   for all tested conditions, the power output will be lower, as a result of the lower number of
325   cations, diffusing through the membrane and reacting with the incoming electrons. This is also
326   reflected by the fact that the terracotta based MEAs reached maximum power output just after
327   5 days of operation[42] whereas the other materials needed more time to reach that. The next
328   five days continued with daily anolyte exchanges of 25 mL fresh urine as indicated by the
329   spikes on the graph. During this period, the MFCs showed consistent increase in power output
330   with a peak at 75 µW for air-dry clay followed by terracotta and air-dry Fimo™, which were
331   almost on a par at 58 µW and 54 µW, respectively; the CEM was the least performing with 37
332   µW. Nine days after the start of the experiment and the daily complete emptying and refilling
333   of the anode chambers with fresh organic matter, the mode of feeding was switched to 5 mL
334   top-ups, after manually removing the same liquid volume from each anode. This had as an
335   impact the overall increase in power output of the MFCs by 11%-15%, however performance
336   would decrease much faster due to the lower amount of fresh carbon-energy available.
337   Bacteria were presumably still consuming other by-products available in the suspension -
338   within the 24 hour window between each feeding- however the power output at the end of
339   each feeding cycle was consistently at the same level of 40 µW each time. In order to
340   compensate for the impact of each feeding approach on the power performance, it was

decided to have a complete exchange of anolyte early each week, followed by a daily top-up
of 5 mL until the end of the week. This strategy was followed until the end of the experiment.

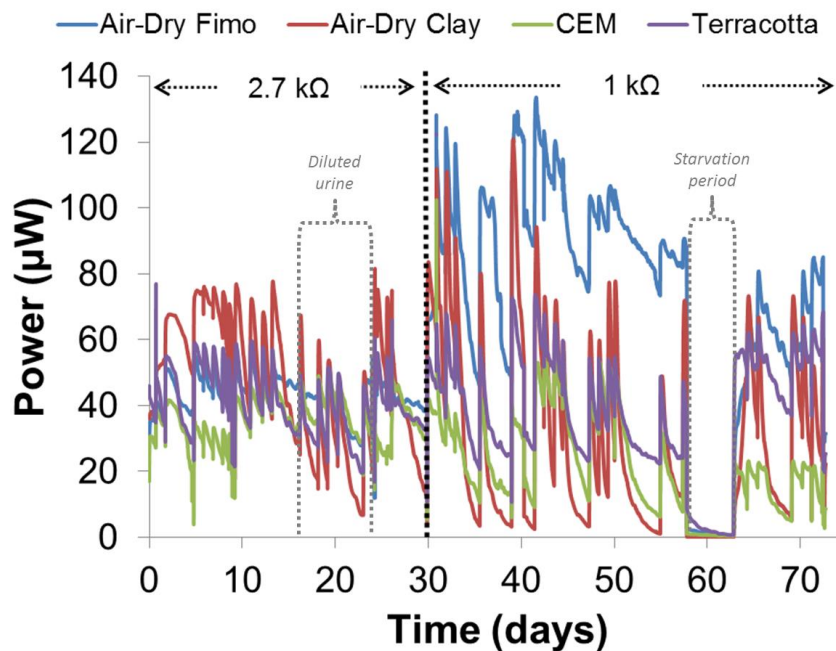### 3.3.2 Long term power output profile of the entire experiment duration

Figure 6. Power generation over 70 days operations

As explained earlier, the experiment was maintained at a constant external load of 2.7 kΩ for
the initial 30 days of operation, during which it was clearly observed that the air-dry clay was
the best performing, while the air-dry Fimo™ and terracotta were on a par; in most cases CEM
was the least performing. Although a steady-state was achieved within the first fifteen days of
operation for all the MFCs, this was lost due to urine shortage and having to use diluted urine
(50:50) between the fifteenth and twenty-fourth day of the experiment (Figure 6). It is
envisaged that the steady state was going to be continued at the same levels if neat urine had
been supplied to the bacteria. This hypothesis is confirmed by the data of the twenty-fifth day
where the output of the MFCs recovered to the previous levels once un-diluted neat urine was
supplied. Following a month of operation at a constant load, the MFCs were subjected to
polarization using an automated Resistorstat as explained previously (Section 2.6) in order to
identify the optimum resistance value based on each system that can give the maximum power
output. Although the polarization results are discussed in detail below (Section 3.2), the impact
of identifying and applying the optimum external load on the MFCs will be discussed here. The
results of the polarization experiment showed that those particular MFC systems can operate
at their best when they are subjected to an external loading of 1 kΩ resistance. Once the
external resistance switched to 1 kΩ, Fimo™ outperformed the rest and the overall power
output of all others also increased by 25%-50%. The performance of the MFCs was
maintained at the same levels for the following month until a complete starvation of four
consecutive days brought all the systems to nearly zero (from day 58 to day 62). During this
period, all the anode MFC chambers completely dried out from evaporation (Figure 6).
However, once the MFCs were fed again, the bacterial communities of the already established
anode biofilm switched from inactive mode (carbon limited) to active mode. Therefore, the
power performance recovered immediately back to similar levels as those from the last

369   feeding. More specifically, Fimo™ separated MFCs reached 91.25% recovery, air-dry clay
370   and CEM reached full recovery (100%), while interestingly terracotta separated MFCs had an
371   increase of 13.4%. However compared to the highest levels of performance recorded during
372   days 30-45, the percentage of recovery was 63.5%, 64%, 40.5% and 91% for Fimo™, air-dry
373   clay, CEM and terracotta respectively. The recovery profile of the previously dried and inactive
374   MFCs adds an extra value to the feasibility of those systems. MFCs are biological entities that
375   not only have long-term power production capabilities -for as long as organic matter is
376   supplied- but more importantly, can survive elongated periods of starvation with demonstrable
377   fast response/recovery. In addition, inexpensive materials such as air-dry clays and terracotta
378   can be used to make these MFCs, which is an economic advantage over traditional
379   commercially available ion exchange membranes.
380
381   **3.3.3   Polarization results**
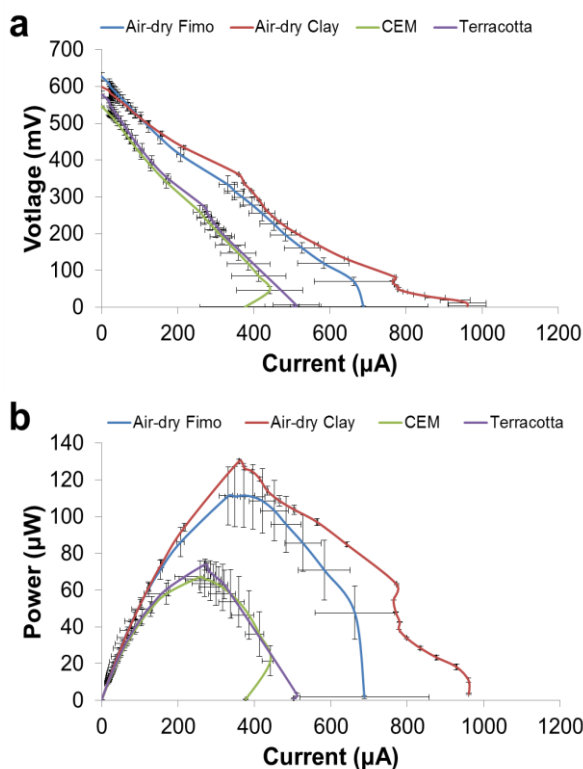
Figure 7. Polarization results a) voltage vs current curve and b) power curve.
Error bars are shown for all conditions

382

383   After a whole month of operation under a constant load (2.7 kΩ), all the MFCs were subjected
384   to polarization analysis by sweeping the external resistance value in a gradual manner starting
385   from infinite resistance (open circuit) and finishing at a very low resistance value (heavy load).
386   Throughout the polarization experiment, the voltage output of the cells was recorded as a
387   function of resistance, which made it possible for the automated system to calculate the
388   current and subsequently the power output. Using the aforementioned data a polarization
389   curve (Figure 7.A) was generated by plotting the voltage versus current. The recordings from
390   each triplicate of MFCs were averaged and plotted including the standard deviations. The
391   initial values at 1MΩ resistance (no current) show the open circuit voltage (OCV) of all the
392   cells at around 600±50 mV. The OCV of the tested MFCs was around 500 mV below the

393 theoretical OCV value (1.1 V) for open-to-air cathode MFCs primarily due to activation
394 overpotentials, which is a characteristic of MFCs with air-breathing cathodes, which operate
395 on the oxygen reduction reaction (ORR); this is limiting when occurring in neutral media [22].
396 These OCV values are in agreement with other open-to-air MFC devices under similar
397 operating conditions [13,46]. Although in the literature there are also higher OCV values
398 reported (0.7-1.0 V), the cathode electrodes of those MFCs were either supplemented with
399 ferricyanide, during the polarization experiment, or were moistened continuously with tap
400 water [47–49].

401 The scope of the polarization experiment is to understand better the specific characteristics of
402 the systems under examination in order to measure their power outputs. Figure 7.B shows the
403 power curves generated, this graph gives us the possibility to assess the maximum power
404 transfer point (MPP), which is the maximum peak of each power curve and corresponds to the
405 optimum resistance value that can give this output. Based on the results, it is evident that air-
406 dry clay had the highest power output at 130 µW followed by air-dry Fimo™ with 111 µW.
407 These results were in accordance with the real time data of the initial thirty days shown above
408 (Section 3.3.2) proving that the air-dry membranes generated the highest amount of power
409 output. The two underperforming MFCs were the control ones with terracotta (73 µW) and
410 CEM giving 50% less than the air-dry clay (66 µW).

411 Comparing the power density of the MFCs reported herein with other MEA-based MFCs in the
412 literature, the 3D-printable ones are showing promising results. In particular a study on tubular
413 MFCs with air breathing cathodes based on CEM-MEA had a power density of 5W m^{-3} (based
414 on the anodic liquid volume of 200 mL) [50]. This output is 0.2 W m^{-3} less than the air-dry clay-
415 MEA of this study, calculated based on a reactor volume of 25 mL. Additionally apart from the
416 advantage over the power density, the MEA used in the aforementioned study [49] was
417 fabricated using carbon cloth coated with a mixture of Pt powder and carbon black bonded
418 together with Nafion resin, which inherently increases the cost.

419 Following polarization analysis, the optimal external resistance was identified (1 kΩ). Once the
420 MFCs were connected to this lower resistance value, the performance levels begun to diverge
421 and Fimo™ was producing the highest power output as can be seen in Figure 6. Although
422 after the change in external resistance, the results of the polarization differed from the real-
423 time data (day 30 onwards) and Fimo™ ended up outperforming the air-dry, in all cases the
424 soft materials were operating better than the conventional cation exchange membrane.

425 **3.4 COD Analysis**

426 Following the increase in performance due to the external loading shift, a chemical oxygen
427 demand (COD) analysis was conducted to observe the rate of COD decrease within a 24 hour
428 period. On the eleventh day following the switch in external resistance (forty-second day of
429 the entire experiment), prior to replenishing the anode chamber with the 25 mL of urine a
430 sample was taken for COD analysis. In parallel to that, a sample from that urine (25 mL) was
431 kept in a closed glass bottle on the bench to observe the decrease in COD without being
432 treated in MFC. The following day, a sample of the effluent of all the MFCs was taken and
433 analysed. The results of this analysis are presented in Figure 8.A. which shows that MFCs
434 with air-dry Fimo™ MEA had a decrease of almost 82±1% in COD which was 4% higher than
435 air-dry clay and terracotta. CEM based MFCs resulted in 63±1% COD decrease. The control
436 COD reduction occurring in the closed glass bottle after 24 hours was 4.7%; this value was

deducted from the overall percentage decreases of all MFCs. This was in order to demonstrate the decrease in COD, which was induced due to the bioelectrocatalytic activity of the electroactive microorganisms presented in the anode and also by fermentative floating microorganisms.
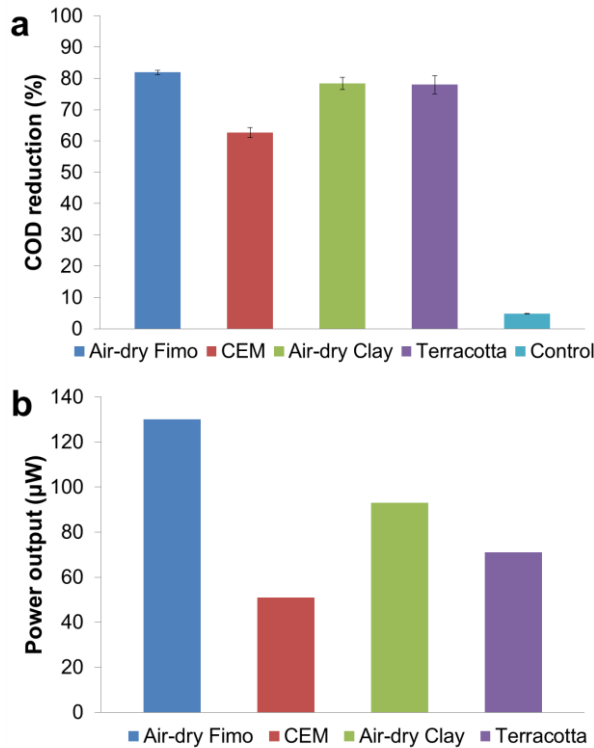
Figure 8. COD reduction results and power output at the time of sampling. a) Percentage of COD reduction of fresh urine within 24 hours in an MFC and in a closed glass bottle (control). b). Power Output of the MFCs at the moment that the samples for COD analysis were taken.

The results of the COD analysis are in agreement with the real time data of that period (day 42), which confirm and support the literature which reports that the highest the power output the highest the COD removal [51]. For clarity Figure 8.B shows the power output of the MFCs at the time that the samples were taken. Based on that in terms of power output Fimo™ was at 130 µW, air-dry clay and terracotta performed 29% and 45% lower than Fimo™ whereas CEM had a 60% less power output than the aforementioned (51 µW). Figure 8 demonstrates clearly the correlation of power output to COD reduction and adds an extra value to the feasibly of those MEAs as alternative conductive separators of MFCs.

The capability of MFCs in treating wastewater and pollutants [52–54] while generating electricity is one of the attractive characteristics of the technology that make it a favourable off-grid source of electricity and sanitation.

3.5 Cost Analysis

As microbial fuel cell is a technology producing low quantity of electricity, particular attention needs to be given to the overall cost needed in maximizing the performance while minimizing

457 the costs. In this section, the cost of the membranes is illustrated and discussed (Figure 9).
458 The cost of the ceramic membranes was calculated considering 1 kilo of raw materials. More
459 specifically, at the moment of purchase air-dry Fimo™ cost 4.94 £ kg^{-1}, air-dry clay cost 3.75
460 £ kg^{-1} while terracotta was the least expensive of all as it was 33% cheaper than air-dry clay
461 and roughly 50% cheaper than air-dry Fimo™. The cost of the latter was in fact 2.52 £ kg^{-1}.
462 The CEM cost was considered to be 188 £ m^{-2}(250$ m^{-2}) according to the supplier. Each
463 membrane was weighed during fabrication and therefore the composition was known. In the
464 case of CEM, a total area of 25 cm^{-2} was used. In order to fabricate the ceramic membranes,
465 6 g, 8 g and 10 g of air-dry Fimo™, air-dry clay and terracotta respectively were used.
466 Consequently, the overall cost for each membrane (with an area of 25 cm^{-2}) was similar for
467 air-dry Fimo™ and air-dry clay at £0.030 per membrane and terracotta being slightly lower at
468 £0.025 per membrane mainly due to the lower cost of the raw material. CEM was the most
469 expensive costing £0.78 per membrane (Figure 9.A). This means that it is possible to fabricate
470 26 air-dry Fimo™/air-dry clay membranes or 31 terracotta membranes for every single CEM
471 membrane for the same cost.
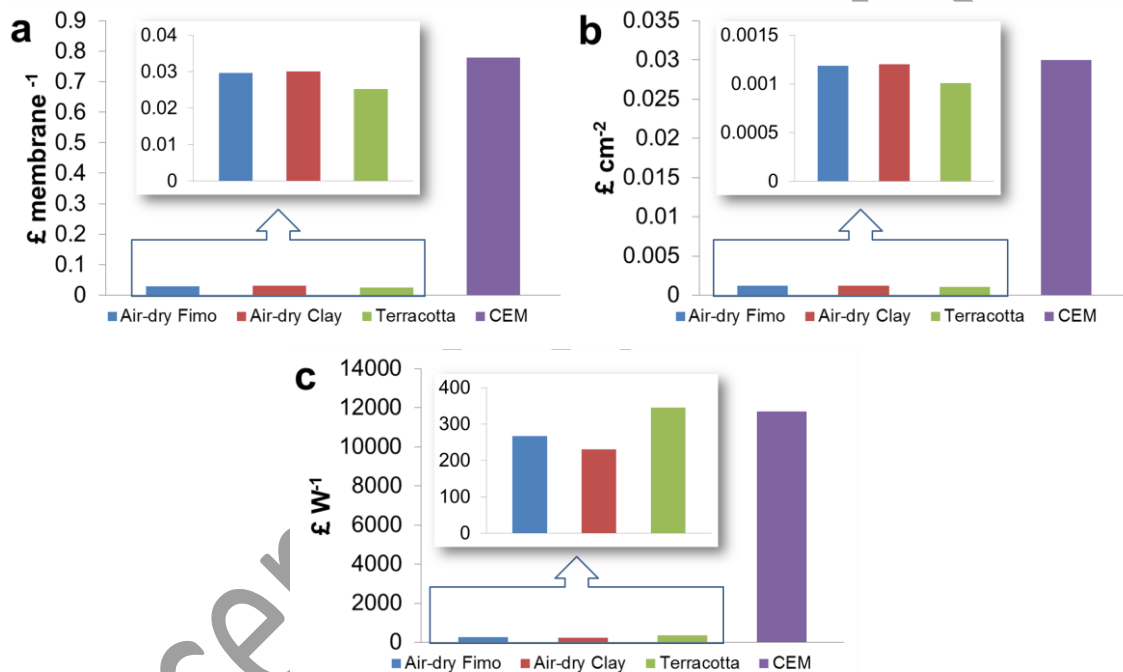
Figure 9. Cost analysis of the membranes. a) Overall cost of the membranes, b) cost of
the membrane for unit of area c) and cost of the membrane for unit of power produced.

472 Another important aspect to consider is the cost of the membrane density meaning the cost of
473 the membrane per cm^2. The results are shown in Figure 9.B. The trend reflects the cost of the
474 raw materials with terracotta having the lowest cost per surface area and CEM the highest.
475 Particularly, the cost for terracotta was roughly 0.1 pence per cm^2 (10£ cm^{-2}) followed by air-
476 dry Fimo™ and air-dry clay with a cost of roughly 0.12 pence per cm^2 (12 £ m^{-2}) and CEM
477 thirty times higher than that (≈300 £ m^{-2}).

478 Finally, the cost of membrane for each Watt produced was also calculated (Figure 9.C). The
479 power from the peak of power curves (Figure 7.B) was considered in 130 µW, 111 µW, 73 µW
480 and 60 µW for air-dry clay, air-dry Fimo™, terracotta and CEM respectively. Due to the higher
481 performance, air-dry clay had the higher value of cost per power produced among the
482 materials investigated that was quantified in 230 £ W^{-1} (Figure 9.C). Slightly higher value was

483   achieved by air-dry Fimo™ with 267 £ W^{-1}. Terracotta had a cost per W produced of 345 £ W^{-1}
484   ^{1} and CEM had an astonishing value of 11818 £ W^{-1}. The cost per W produced of CEM was
485   34, 44, 51 times higher compared to terracotta, air-dry Fimo™ and air-dry clay respectively.
486   Among the three clay-based membranes, the most cost-effective material tested was air-dry
487   clay. The cost per W produced was 14% and 33% better compared to air-dry Fimo™ and
488   terracotta respectively. Air-dry Fimo™, air-dry clay and terracotta seems to be very promising
489   cost-effective membranes materials that can replace the more expensive and not
490   environmentally-friendly polymeric membranes. It must be noted that the cost of kilning or
491   shipping from abroad were not taken into account for these economic calculations.

492   **3.6   3D-printing MEAs using EvoBot.**

493   EvoBot (Figure 10.A) is a RepRap open-source 3D-printer modified successfully to operate
494   like a robot for culturing and maintaining Microbial Fuel Cells (MFCs) based on an established
495   feedback loop between the MFC systems and the python controlled platform [55]. EvoBot can
496   host a large number of MFCs (24) on its experimental arena where it can gather data about
497   the MFCs and react through a feedback loop to set thresholds (voltage output). This improves
498   the performance of the MFCs by providing nutrient supply only when needed. So far this type
499   of liquid handling robot-MFC interaction, based on the feedback loop mechanism, has enabled
500   the study the adaptability and stability of those systems [55].

501   Since EvoBot is a 3D-printer turned to robot it still holds its 3D-printing capabilities thus it can
502   extrude (3D-print) parts for MFCs with the ultimate aim to monolithically print and nurture those
503   already made MFCs. Having this in mind, the two air-dry materials tested as alternative
504   membranes -against conventional polymeric cation exchange membranes and fired
505   terracotta- come in the form of soft modelling clay, which makes them suitable for extrusion
506   from the EvoBot platform (Figure 10.B). As the uncured form of the electrode material is also
507   fluid, it can be applied using EvoBot by incorporating a brush/roller on the actuation layer of
508   the robot. This will apply the conductive coating onto the dried extruded membranes.

Figure 10. EvoBot Rep-Rap 3D-printer. a) EvoBot within is Evo-world enclosure performing experiments on MFCs under controlled conditions b) EvoBot with an adapted extruder 3D-prints Fimo™ membranes. Source: www.evobliss-project.eu.

509

510 ### 3.7 Conclusions

511 This study explored the idea of using air-dry based materials such as Fimo™ and clay to
512 fabricate membrane electrode assemblies for Microbial Fuel Cells (MFC) which were then
513 compared against two of the most popularly used materials in the field, cation exchange
514 membrane (CEM) and kilned red terracotta. Through this study it has been successfully shown
515 that MFCs with air-dry clay based MEAs can produce up to 50% more power than the controls.
516 Since the MFC technology relies on low-cost materials, due to the small amount of electricity
517 generated per MFC unit, the fact that terracotta, air-dry Fimo™ and air-dry clay were 40±10
518 times cheaper than CEM (per Watt produced), adds an extra advantage in using these
519 materials. In addition those MFCs had a COD reduction of nearly 80% which was 20% more
520 than what the CEM based MFCs achieved. At last, the capabilities of those air-cured materials
521 open another promising avenue to the MFC research as their fabrication can be done with 3D
522 printing and/or extrusion techniques using the EvoBot platform. Thus it is envisaged that
523 monolithically 3D-printed MFCs are feasible and can potentially emerge from platforms such
524 as EvoBot.

525 ### Acknowledgments

532 ### References

533 [1]   International Energy Agency. World Energy Outlook 2017. OECD; 2017.
534   doi:10.1787/weo-2017-en.

535 [2]   Potter M. Electrical Effects Accompanying the Decomposition of Organic Compounds
536   Published by : The Royal Society Electrical Effects accompanying the Decormposition
537   of Organic. Proc R Soc London Ser B, Contain Pap a Biol Character, 1911;84:260–
538   76.

539 [3]   Allen RM, Bennetto HP. Microbial fuel-cells: Electricity Production from
540   Carbohydrates. Appl Biochem Biotechnol 1993;39:27–40.

541 [4]   Bennetto HP. Electricity generation by microorganisms. Biotechnol Educ 1990;1:163–
542   8.

543 [5]   Jung S, Regan JM. Comparison of anode bacterial communities and performance in
544   microbial fuel cells with different electron donors. Appl Microbiol Biotechnol
545   2007;77:393–402. doi:10.1007/s00253-007-1162-y.

546 [6]   Hassan SHA, Gad El-Rab SMF, Rahimnejad M, Ghasemi M, Joo JH, Sik-Ok Y, et al.
547   Electricity generation from rice straw using a microbial fuel cell. Int J Hydrogen Energy
548   2014;39:9490–6. doi:10.1016/j.ijhydene.2014.03.259.

549 [7]   Bennetto H, Mason JR, Stirling JL, Thurston CF. Miniature microbial biobatteries.
550   Power Sources 1987;11:373–380.

551 [8]   Du Z, Li H, Gu T. A state of the art review on microbial fuel cells: A promising
552   technology for wastewater treatment and bioenergy. Biotechnol Adv 2007;25:464–82.
553   doi:10.1016/j.biotechadv.2007.05.004.

554 [9]   Ieropoulos IA, Stinchcombe A, Gajda I, Forbes S, Merino-Jimenez I, Pasternak G, et
555   al. Pee power urinal – microbial fuel cell technology field trials in the context of
556   sanitation. Environ Sci Water Res Technol 2016;2:336–43.
557   doi:10.1039/C5EW00270B.

558 [10]   Papaharalabos G, Greenman J, Melhuish C, Ieropoulos I. A novel small scale
559   Microbial Fuel Cell design for increased electricity generation and waste water
560   treatment. Int J Hydrogen Energy 2015;40:4263–8.
561   doi:10.1016/j.ijhydene.2015.01.117.

562 [11]   Ieropoulos I, Greenman J, Melhuish C. Microbial fuel cells based on carbon veil
563   electrodes: Stack configuration and scalability. Int J Energy Res 2008;32:1228–40.
564   doi:10.1002/er.1419.

565 [12]   Wei J, Liang P, Huang X. Recent progress in electrodes for microbial fuel cells.
566   Bioresour Technol 2011;102:9335–44. doi:10.1016/j.biortech.2011.07.019.

567 [13]   You J, Santoro C, Greenman J, Melhuish C, Cristiani P, Li B, et al. Micro-porous layer
568   (MPL)-based anode for microbial fuel cells. Int J Hydrogen Energy 2014;39:21811–8.
569   doi:10.1016/j.ijhydene.2014.07.136.

570 [14]   Guerrini E, Grattieri M, Trasatti SP, Bestetti M, Cristiani P. Performance explorations
571   of single chamber microbial fuel cells by using various microelectrodes applied to
572   biocathodes. Int J Hydrogen Energy 2014;39:21837–46.
573   doi:10.1016/J.IJHYDENE.2014.06.132.

574 [15]   Santoro C, Agrios A, Pasaogullari U, Li B. Effects of gas diffusion layer (GDL) and
575   micro porous layer (MPL) on cathode performance in microbial fuel cells (MFCs). Int J
576   Hydrogen Energy 2011;36:13096–104. doi:10.1016/j.ijhydene.2011.07.030.

577 [16] Chaudhuri SK, Lovley DR. Electricity generation by direct oxidation of glucose in
578   mediatorless microbial fuel cells. Nat Biotechnol 2003;21:1229–32.
579   doi:10.1038/nbt867.

580 [17] Aelterman P, Versichele M, Marzorati M, Boon N, Verstraete W. Loading rate and
581   external resistance control the electricity generation of microbial fuel cells with
582   different three-dimensional anodes. Bioresour Technol 2008;99:8895–902.
583   doi:10.1016/j.biortech.2008.04.061.

584 [18] Santoro C, Guilizzoni M, Correa Baena JP, Pasaogullari U, Casalegno A, Li B, et al.
585   The effects of carbon electrode surface properties on bacteria attachment and start up
586   time of microbial fuel cells. Carbon N Y 2014;67:128–39.
587   doi:10.1016/j.carbon.2013.09.071.

588 [19] Santoro C, Artyushkova K, Gajda I, Babanova S, Serov A, Atanassov P, et al.
589   Cathode materials for ceramic based microbial fuel cells (MFCs). Int J Hydrogen
590   Energy 2015;40:14706–15. doi:10.1016/j.ijhydene.2015.07.054.

591 [20] Merino-Jimenez I, Santoro C, Rojas-Carbonell S, Greenman J, Ieropoulos I,
592   Atanassov P. Carbon-Based Air-Breathing Cathodes for Microbial Fuel Cells.
593   Catalysts 2016;6:127. doi:10.3390/catal6090127.

594 [21] Wang Z, Mahadevan GD, Wu Y, Zhao F. Progress of air-breathing cathode in
595   microbial fuel cells. J Power Sources 2017;356:245–55.
596   doi:10.1016/j.jpowsour.2017.02.004.

597 [22] Santoro C, Arbizzani C, Erable B, Ieropoulos I. Microbial fuel cells: From
598   fundamentals to applications. A review. J Power Sources 2017;356:225–44.
599   doi:10.1016/j.jpowsour.2017.03.109.

600 [23] Sealy C. The problem with platinum. Mater Today 2008;11:65–8. doi:10.1016/S1369-
601   7021(08)70254-2.

602 [24] Ieropoulos I, Winfield J, Gajda I, Walter A, Papaharalabos G, Jimenez IM, et al. The
603   Practical Implementation of Microbial Fuel Cell Technology. Elsevier Ltd.; 2015.
604   doi:10.1016/B978-1-78242-375-1.00012-5.

605 [25] Yang W, Li J, Zhang L, Zhu X, Liao Q. A monolithic air cathode derived from bamboo
606   for microbial fuel cells. RSC Adv 2017;7:28469–75. doi:10.1039/c7ra04571a.

607 [26] Yang W, Li J, Ye D, Zhu X, Liao Q. Bamboo charcoal as a cost-effective catalyst for
608   an air-cathode of microbial fuel cells. Electrochim Acta 2017;224:585–92.
609   doi:10.1016/j.electacta.2016.12.046.

610 [27] Zhang Y, Yang W, Fu Q, Li J, Zhu X, Liao Q. Performance optimization of microbial
611   fuel cells using carbonaceous monolithic air-cathodes. Int J Hydrogen Energy 2018:1–
612   7. doi:10.1016/j.ijhydene.2018.07.132.

613 [28] Walter XA, Gajda I, Forbes S, Winfield J, Greenman J, Ieropoulos I. Scaling-up of a
614   novel, simplified MFC stack based on a self-stratifying urine column. Biotechnol
615   Biofuels 2016;9:93. doi:10.1186/s13068-016-0504-3.

616 [29] Harnisch F, Schröder U. Selectivity versus mobility: Separation of anode and cathode
617   in microbial bioelectrochemical systems. ChemSusChem 2009;2:921–6.
618   doi:10.1002/cssc.200900111.

619 [30] Ghasemi M, Wan Daud WR, Ismail M, Rahimnejad M, Ismail AF, Leong JX, et al.
620   Effect of pre-treatment and biofouling of proton exchange membrane on microbial fuel

621   cell performance. Int J Hydrogen Energy 2013;38:5480–4.
622   doi:10.1016/j.ijhydene.2012.09.148.

623 [31] Flimban SGA, Hassan SHA, Rahman MM, Oh SE. The effect of Nafion membrane
624   fouling on the power generation of a microbial fuel cell. Int J Hydrogen Energy
625   2018:1–9. doi:10.1016/j.ijhydene.2018.02.097.

626 [32] Xu J, Sheng GP, Luo HW, Li WW, Wang LF, Yu HQ. Fouling of proton exchange
627   membrane (PEM) deteriorates the performance of microbial fuel cell. Water Res
628   2012;46:1817–24. doi:10.1016/j.watres.2011.12.060.

629 [33] Winfield J, Gajda I, Greenman J, Ieropoulos I. A review into the use of ceramics in
630   microbial fuel cells. Bioresour Technol 2016;215:296–303.
631   doi:10.1016/j.biortech.2016.03.135.

632 [34] Yousefi V, Mohebbi-Kalhori D, Samimi A. Ceramic-based microbial fuel cells (MFCs):
633   A review. Int J Hydrogen Energy 2017;42:1672–90.
634   doi:10.1016/j.ijhydene.2016.06.054.

635 [35] Nandy A, Kumar V, Mondal S, Dutta K, Salah M, Kundu PP. Performance evaluation
636   of microbial fuel cells: Effect of varying electrode configuration and presence of a
637   membrane electrode assembly. N Biotechnol 2015;32:272–81.
638   doi:10.1016/j.nbt.2014.11.003.

639 [36] Faíña A, Nejatimoharrami F, Stoy K, Theodosiou P, Taylor B, Ieropoulos I. EvoBot :
640   An Open-Source , Modular Liquid Handling Robot for Nurturing Microbial Fuel Cells.
641   Proc. Artif. Life Conf. 2016, 2016, p. 626–33.

642 [37] Ieropoulos I, Theodosiou P, Taylor B, Greenman J, Melhuish C. Gelatin as a
643   promising printable feedstock for microbial fuel cells (MFC). Int J Hydrogen Energy
644   2017;42:1783–90. doi:10.1016/j.ijhydene.2016.11.083.

645 [38] Winfield J, Chambers LD, Stinchcombe A, Rossiter J, Ieropoulos I. The power of
646   glove: Soft microbial fuel cell for low-power electronics. J Power Sources
647   2014;249:327–32. doi:10.1016/j.jpowsour.2013.10.096.

648 [39] Clinton DJ, Morrell R. Hardness testing of ceramic materials. Mater Chem Phys
649   1987;17:461–73. doi:10.1016/0254-0584(87)90096-4.

650 [40] Degrenne N, Buret F, Allard B, Bevilacqua P. Electrical energy generation from a
651   large number of microbial fuel cells operating at maximum power point electrical load.
652   J Power Sources 2012;205:188–93. doi:10.1016/j.jpowsour.2012.01.082.

653 [41] Winfield J, Ieropoulos I, Greenman J, Dennis J. The overshoot phenomenon as a
654   function of internal resistance in microbial fuel cells. Bioelectrochemistry 2011;81:22–
655   7. doi:10.1016/j.bioelechem.2011.01.001.

656 [42] Pasternak G, Greenman J, Ieropoulos I. Comprehensive Study on Ceramic
657   Membranes for Low-Cost Microbial Fuel Cells. ChemSusChem 2016;9:88–96.
658   doi:10.1002/cssc.201501320.

659 [43] Rossiter J, Winfield J, Ieropoulos I. Here today, gone tomorrow: biodegradable soft
660   robots 2016;9798:97981S. doi:10.1117/12.2220611.

661 [44] Kaiyu Industrial LTD. Micronized Graphite 2018.
662   http://www.kyugraphite.com/micronized-graphite-3276941.html.

663 [45] Winfield J, Chambers LD, Rossiter J, Greenman J, Ieropoulos I. Urine-activated

664   origami microbial fuel cells to signal proof of life. J Mater Chem A 2015;3:7058–65.
665   doi:10.1039/C5TA00687B.

666 [46] Papaharalabos G, Greenman J, Melhuish C, Santoro C, Cristiani P, Li B, et al.
667   Increased power output from micro porous layer (MPL) cathode microbial fuel cells
668   (MFC). Int J Hydrogen Energy 2013;38:11552–8. doi:10.1016/j.ijhydene.2013.05.138.

669 [47] Logan B. Microbial Fuel Cells. Hoboken, New Jersey: John Wiley & Sons; 2008.

670 [48] Ieropoulos I, Greenman J, Melhuish C. Improved energy output levels from small-
671   scale Microbial Fuel Cells. Bioelectrochemistry 2010;78:44–50.
672   doi:10.1016/j.bioelechem.2009.05.009.

673 [49] Ieropoulos I, Melhuish C, Greenman J. Artificial gills for robots: MFC behaviour in
674   water. Bioinspir Biomim 2007;2:S83–93. doi:10.1088/1748-3182/2/3/S02.

675 [50] Kim JR, Premier GC, Hawkes FR, Dinsdale RM, Guwy AJ. Development of a tubular
676   microbial fuel cell (MFC) employing a membrane electrode assembly cathode. J
677   Power Sources 2009;187:393–9. doi:10.1016/j.jpowsour.2008.11.020.

678 [51] Zhang X, He W, Ren L, Stager J, Evans PJ, Logan BE. COD removal characteristics
679   in air-cathode microbial fuel cells. Bioresour Technol 2015;176:23–31.
680   doi:10.1016/j.biortech.2014.11.001.

681 [52] Ahn Y, Logan BE. Effectiveness of domestic wastewater treatment using microbial
682   fuel cells at ambient and mesophilic temperatures. Bioresour Technol 2010;101:469–
683   75. doi:10.1016/j.biortech.2009.07.039.

684 [53] Gajda I, Greenman J, Melhuish C, Ieropoulos IA. Electricity and disinfectant
685   production from wastewater: Microbial Fuel Cell as a self-powered electrolyser. Sci
686   Rep 2016;6:25571. doi:10.1038/srep25571.

687 [54] Liu Y, Liu H, Wang C, Hou SX, Yang N. Sustainable energy recovery in wastewater
688   treatment by microbial fuel cells: Stable power generation with nitrogen-doped
689   graphene cathode. Environ Sci Technol 2013;47:13889–95. doi:10.1021/es4032216.

690 [55] Theodosiou P, Faina A, Nejatimoharrami F, Stoy K, Greenman J, Melhuish C, et al.
691   EvoBot: Towards a Robot-Chemostat for Culturing and Maintaining Microbial Fuel
692   Cells (MFCs). Biomim. Biohybrid Syst., Springer, Cham; 2017, p. 453–64.
693   doi:10.1007/978-3-319-63537-8_38.

694